



## Calhoun: The NPS Institutional Archive

---

Faculty and Researcher Publications

Faculty and Researcher Publications

---

2000

# Aerosol particle chemical characteristics measured from aircraft in the lower troposphere during ACE-2

Schmeling, Martina

---



Calhoun is a project of the Dudley Knox Library at NPS, furthering the precepts and goals of open government and government transparency. All information contained herein has been approved for release by the NPS Public Affairs Officer.

**Dudley Knox Library / Naval Postgraduate School**  
**411 Dyer Road / 1 University Circle**  
**Monterey, California USA 93943**

<http://www.nps.edu/library>

## Aerosol particle chemical characteristics measured from aircraft in the lower troposphere during ACE-2

By MARTINA SCHMELING<sup>1</sup>, LYNN M. RUSSELL<sup>1\*</sup>, CARYNELISA ERLICK<sup>2</sup>, DONALD R. COLLINS<sup>3</sup>, HAFLIDI JONSSON<sup>4</sup>, QING WANG<sup>4</sup>, PETER KREGSAMER<sup>5</sup> and CHRISTINA STRELI<sup>6</sup>, <sup>1</sup>*Department of Chemical Engineering, Princeton University, Princeton, New Jersey;* <sup>2</sup>*Atmospheric and Oceanic Sciences Program, Princeton University, Princeton, New Jersey;* <sup>3</sup>*Department of Chemical Engineering, California Institute of Technology, Pasadena, California;* <sup>4</sup>*Department of Meteorology, Naval Postgraduate School, Monterey, California, USA;* <sup>5</sup>*Atominstitut of the Austrian Universities, Vienna, Austria*

(Manuscript received 7 January 1999; in final form 13 September 1999)

### ABSTRACT

During the Aerosol Characterization Experiment (ACE-2), filter samples were collected aboard the Center for Interdisciplinary Remotely Piloted Aircraft Studies (CIRPAS) Pelican aircraft near Tenerife in June and July of 1997. The flights included constant altitude measurements in the boundary layer as well as profiles up to 3800 m providing detailed chemical information about the composition of the aerosol distribution in the lower troposphere. Three cases with different air mass origins — clean marine air, anthropogenically-influenced air from the European continent, and dust-laden air from the Sahara — were identified. The samples were analyzed by ion chromatography (IC) for ionic species, by combined thermal and optical analysis (TOA) for organic carbon, and by total reflection X-ray fluorescence (TXRF) for elemental composition. Particle composition and size distributions for the range of air masses encountered illustrate links in the chemical and microphysical characteristics of aerosol from different sources. Clean marine air masses were characterized by low particle number and mass concentrations with no detectable metals, while anthropogenically-influenced and dust-laden air had high number, mass, and trace metal concentrations. Anthropogenic sources were characterized by high concentrations of submicron particles and some Fe and Cu, whereas dust particle loadings included a significant mass of micron-sized particles and significant loadings of Fe, in addition to small amounts of Mn, Cu, and Ni. These results showed similar tracers for air mass origin as those found in other measurements of oceanic and continental air masses. Aerosol optical properties were estimated with a simplified model of the aerosol based on the measured compositions. The real and imaginary refractive indices and single scattering albedos differed significantly among the three types of aerosol measured, with clean marine aerosol properties showing the least absorption and dust-containing aerosols showing the most. There were only small differences in optical properties for the two different cases of clean marine aerosol, but some significant differences between the two dust cases. Since measurement uncertainties affect these calculations, we studied the type of mixing and the fraction of absorbing species and found the calculation was sensitive to these variations only for the dust-containing aerosol case, probably due to the small amount of water present. While the optical properties varied little

---

\* Corresponding author: A317 Engineering  
Quadrangle, Princeton University, Princeton,  
NJ 08544, USA.  
email: lrussell@princeton.edu.

with composition for clean marine and anthropogenically-influenced cases, they showed a strong dependence on variations in particle composition and mixing state for the dust-containing cases.

## 1. Introduction

Aerosol properties in the North Atlantic region include a variety of aerosol types, resulting from influences from several different kinds of air masses (Huebert et al., 1996; Russell et al., 1996a). Clean marine air, including air masses from Arctic regions, contains aerosol that has been processed under pristine conditions for several days (Hoppel et al., 1990). Anthropogenically-influenced air masses that originate in Europe frequently include high particle concentrations in the boundary layer from continental sources. Saharan air masses, originating in northern Africa, contain dust particles that have been lifted above the boundary layer by updrafts, providing long-lived and distinctive aerosol layers in the free troposphere (Bergametti et al., 1989; Arimoto et al., 1995). Aerosol chemical composition, particle size distributions, and air mass back trajectories can serve as tracers for the origin of the air mass sampled (Zhang et al., 1993; 1998). Differing particle origins result in mixtures of chemical species with different optical properties (d'Almeida et al., 1991).

During the second Aerosol Characterization Experiment (ACE-2) in the northeastern Atlantic Ocean, a series of aircraft and surface-based measurements was conducted in order to study the chemical and physical properties of the aerosol found in this region of the world (Raes et al., 2000; Verver et al., 2000). Suites of microphysical instrumentation on several platforms measured radiative and microphysical properties of the aerosol particles to quantify their contribution to the so-called direct effect of aerosol on radiative transfer in the atmosphere (Russell and Heintzenberg, 2000). Aerosol filter samples were collected on the CIRPAS Pelican aircraft as well as on several surface and ship-based sites to identify chemical species contributing to optical properties of the aerosol measured (Putaud et al., 2000; Swietlicki et al., 2000; Quinn et al., 2000).

Here, we present the analysis of elemental and ionic species, collected with filter holders aboard the CIRPAS Pelican aircraft near Tenerife. The

Pelican aircraft (a modified Cessna) flew at low-altitude patterns for several hours during some flights, offering the ability to measure aerosol particles in the marine boundary layer. Flight patterns included profiles while descending or climbing in altitude between 50 and 3800 m above sea level to show the vertical variation in the size distribution. The chemical composition provides information about the origin of the air mass. Non-sea salt (nss) sulfate, for example, is an indicator of anthropogenic sources. Trace metal constituents in particles indicate both specific source types and regions (Schütz and Seibert, 1987; Arimoto et al., 1995). The resulting characterization of aerosol sources provides specific examples of the aerosol contribution to scattering and absorbing properties of the atmosphere on local and regional scales.

## 2. Chemical analysis

Samples were collected with a stainless steel filter holder, loaded with 47 mm quartz-fiber filters (2500QAT-UP; Pallflex Products Corp.) that were precleaned by heating at 900 °C, and with a teflon filter holder, loaded with 47 mm teflon filters (Zefluor; Gelman Sciences). Several preferable approaches, including more detailed chemical identification, larger mass collection or multiple size-cut particle impaction were precluded by space, power and sampling time limitations aboard the Pelican aircraft. Quartz-fiber filters were used for collection of organic and elemental carbon and teflon filters for ionic and elemental species. Both filter holders were mounted on the CIRPAS Pelican Aircraft for sampling representative aerosol particles during ACE-2 (Raes et al., 2000; Verver et al., 2000). Sampling times varied between 41 min and 126 min, and air volumes filtered lie in the range of 0.205 m<sup>3</sup> and 0.630 m<sup>3</sup> at a flow rate of 5 l min<sup>-1</sup> for each filter holder. The sampling inlet has a 50% cut-off at approximately 2.5 µm at ambient humidity. Flights included several patterns to sample different regions of the lower troposphere, including some slowly descending profiles to characterize a vertically-

averaged composition in flights 15 and 20, constant-altitude box patterns to provide detailed measurements of the boundary layer on flights 11 and 16, and circles at several altitudes to quantify mixing of aerosol in flight 21.

Elemental (EC) and organic (OC) carbon were identified by thermal-optical analysis (TOA), described by Birch and Carey (1996). In TOA, the aerosol-containing quartz fiber filter is placed in an oven under helium atmosphere and is heated in four increasing temperature steps to a final temperature of 725 °C. Organic carbon volatilizes completely at this temperature and immediately oxidizes to CO<sub>2</sub> on MnO<sub>2</sub>, and then reduces to methane. A flame ionization detector measures the methane concentration evolved by this process. For elemental carbon, the oven is cooled to 850 °C before heating, and the carrier gas is changed to a helium/oxygen mixture in order to oxidize all remaining carbon. Given sufficient loading, elemental carbon can be determined from the difference of total and organic carbon evolved but was below detection by thermal decomposition for the ACE-2 samples. In addition, there was no change in the light fraction reflected in all samples, so that black carbon was also below detection by the simultaneous optical approach used.

Ionic species (Na<sup>+</sup>, Cl<sup>-</sup>, and SO<sub>4</sub><sup>2-</sup>) were analyzed by ion chromatography (IC) (Dionex 2010i, Dionex Corp.), after extraction of the filter with 5 ml of methanol/water (1:10) solution in an ultrasonic bath for at least 6 hr (Huebert et al., 1996). The anion analysis was performed with an AS4 column (Dionex Corp.) and the cation analysis with a CS12A column (Dionex Corp.) under standard conditions.

In addition to ions, elemental species were measured by total reflection X-ray Fluorescence (TXRF), after extraction of the filter with 1 ml hot concentrated nitric acid (Suprapure, EM). In this analysis, 10 µl from each sample was pipetted onto a clean Si-wafer and 3 µl of a 1 µg ml<sup>-1</sup> solution of Cr was added as internal standard for quantification. The droplet was dried under vacuum and irradiated by W-Lβ for 500 s (Schmeling and Klockow, 1997; Strelis, 1997; Klockenkämper, 1997).

In addition to atmospheric samples, blank filters were taken before and after each flight and were handled with the same protocol as the sample filters. Values of blanks for each flight were aver-

aged and subtracted from the measured aerosol mass. Detection limits for each species for the three methods described are presented in Table 1.

Since three main types of air masses are typically found in the Canary Islands — clean marine (flights 11 and 16 on 4 and 9 July, respectively), anthropogenically-influenced (flight 21 on 18 July), and Saharan dust-containing (flights 15 and 20 on 8 and 17 July, respectively) — we will focus here on the distinctive features of the size distributions and chemical compositions of each of these types during ACE-2. Section 3 describes measured chemical compositions and particle size distributions for each of the flights studied. Section 4 compares our results with other measurements that have been reported in the literature for similar and contrasting regions. Chemical composition and size distribution are key factors in determining particle optical properties including refractive indices and single scatter albedo. Section 5 uses the measured compositions to study the sensitivities of these optical properties for each air mass type.

### 3. Aerosol characterization

In Table 1, chemical concentrations obtained for five ACE-2 flights (namely flights 11, 15, 16, 20, and 21) are shown. Figs. 1c, d, 2c, d, and 3b show these values for each component analyzed in each flight. In order to compare the measured composition with the corresponding particle size distribution, we have shown representative size distributions measured from the Automated Classified Aerosol Detector (ACAD, Russell et al., 1996b) for the range 0.005 to 0.190 µm dry diameter and the Passive Cavity Aerosol Spectrometer Probe (PCASP, Particle Measuring Systems, Inc.) for the range 0.1 to 3.0 µm ambient diameter for each flight in Figs. 1a, b, 2a, b, and 3a (Collins et al., 2000). To describe the characteristics for each flight, the particle size distribution has been classified in 3 size categories: Aitken mode particles comprising those particles up to 0.1 µm dry diameter, accumulation mode particles up to 1.0 µm, and coarse mode particles larger than 1.0 µm.

In general, the results for ionic and carbonaceous aerosol are comparable to other measurements made during ACE-2 aboard the R/V

Table 1. Chemical composition of fine aerosol particles measured during ACE-2 Pelican flights

Concentration [ $\mu\text{g}/\text{m}^3$ ]	$\text{SO}_4^{2-\text{a}}$	NSS $\text{SO}_4^{2-\text{a}}$	$\text{OC}^{\text{c}}$	$\text{EC}^{\text{c}}$	$\text{Cl}^{\text{a}}$	Na	Mg <sup>b</sup>	Mn <sup>b</sup>	Fe <sup>b</sup>	Co <sup>b</sup>	Ni <sup>b</sup>	Cu <sup>b</sup>
Detection limits [ $\mu\text{g}$ ]	1.0	1.0	0.20	0.27	3.1	1.7 <sup>a</sup> /0.03 <sup>b</sup>	0.3	0.00002	0.00005	0.00003	0.0001	0.00001
<i>Clean marine cases</i>												
flight 11 (0.50 m <sup>3</sup> )			1.6 $\pm 0.05$	< DL								
flight 16 (0.41 m <sup>3</sup> )	< DL	< DL	1.1 $\pm 0.06$	< DL	1.1 $\pm 0.2$		< DL	< DL	0.333 $\pm 0.002$	< DL	< DL	0.045 $\pm 0.0008$
<i>Dust-containing cases</i>												
flight 15 (0.34 m <sup>3</sup> )			< DL	< DL	< DL	0.11 <sup>b</sup> $\pm 0.01$	5.3 $\pm 0.03$	0.180 $\pm 0.001$	2.95 $\pm 0.05$	0.045 $\pm 0.0007$	0.372 $\pm 0.001$	< DL
flight 20 (0.38 m <sup>3</sup> )	8.6 $\pm 0.20$	6.5	< DL	< DL	< DL	7.8 <sup>a</sup> $\pm 0.4$	< DL	0.036 $\pm 0.0008$	2.58 $\pm 0.06$	< DL	< DL	0.071 $\pm 0.0009$
<i>Anthropogenically-influenced case</i>												
flight 21 (0.42 m <sup>3</sup> )	3.9 $\pm 0.08$	3.8	3.9 $\pm 0.10$	< DL		0.29 <sup>b</sup> $\pm 0.02$	< DL	< DL	0.851 $\pm 0.003$	< DL	< DL	0.108 $\pm 0.001$

The results include analyses by IC, TOA, and TXRF. Blank values indicate that a suitable sample was not available for this element's analysis. "< DL" indicates that no value is reported because the measured value of the sample was below the detection limit of the technique used. Detection limits are reported as total mass of the chemical species required for an individual sample for analysis by (a) ion chromatography (IC), (b) total reflection X-ray fluorescence (TXRF), and (c) thermal-optical analysis (TOA). The corresponding atmospheric loadings can be found by dividing the volume of standard air filtered for each flight, which varied from 0.2 m<sup>3</sup> to 1.9 m<sup>3</sup> during ACE-2.

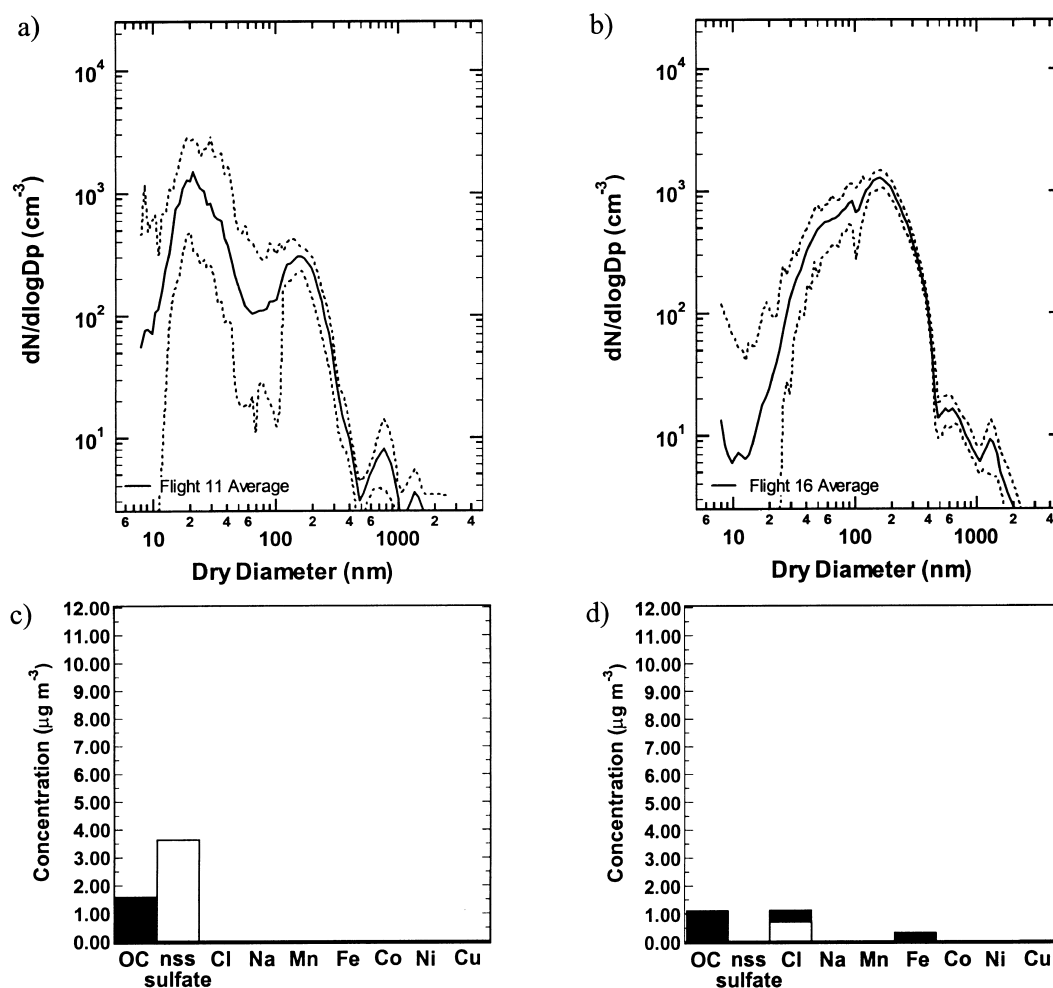


Fig. 1. Aerosol size distributions and chemical compositions for the two clean cases studied, flights 11 and 16. Size distributions from integrated ACAD and PCASP measurements are shown in (a) and (b) for flights 11 and 16. The solid line shows the average value during the filter sampling period for the flight, and the dotted lines give the range of values measured showing the minimum and maximum measured concentrations with size. Chemical composition data are shown in (c) and (d) for flights 11 and 16, respectively. Filled bars indicate measured values, and empty bars are shown to indicate detection limits. For species where no bar is shown, both values are too small to appear in the range of the graph and can be found in Table 1.

Vodyanitskiy and from land-based platforms at Sagres, Portugal, and Punta del Hidalgo, Tenerife (Quinn et al., 2000). The low values of both organic and black carbon in the clean air masses were below detection in many cases for the airborne and ship-based sampling and present below  $0.1 \mu\text{g m}^{-3}$  from ground based data (Quinn et al., 2000). In the more polluted samples, both airborne and surface samples measured concentrations

above  $1 \mu\text{g m}^{-3}$ , although the vertically-averaged flight 21 sample has the highest organic carbon concentration at  $3.9 \mu\text{g m}^{-3}$ , as would be consistent with higher carbonaceous particle loadings aloft. The Na concentration measured varied between 0.1 and  $0.4 \mu\text{g m}^{-3}$  for air, ship and land measurements for all cases except flight 20, where the masses of sulfates, sodium and iron were each above  $2 \mu\text{g m}^{-3}$ . The clean non-seasalt sulfate ion

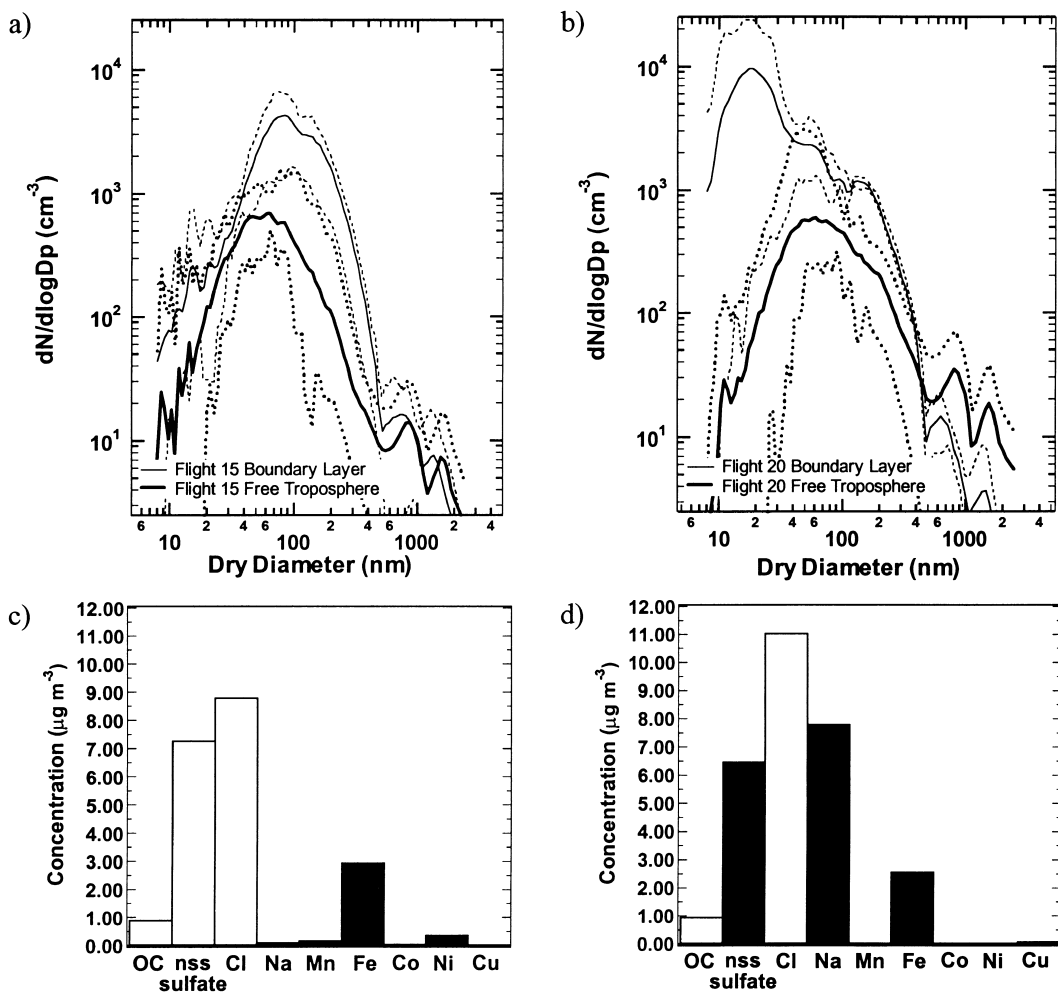


Fig. 2. Aerosol size distributions and chemical compositions for the two dust cases studied, flights 15 and 20. Size distributions from integrated ACAD and PCASP measurements are shown in (a) and (b) for flights 15 and 20, respectively, where thick lines represent the average size distribution above the boundary layer in the free troposphere and thin lines represent the average size distribution in the boundary layer. The solid lines show the average values during the filter sampling period for the two parts of the flight, and the dotted lines give the range of values measured showing the minimum and maximum concentrations with size. Chemical composition data are shown in (c) and (d) for flights 15 and 20, respectively. Filled bars indicate measured values, and empty bars are shown to indicate detection limits. For species where no bar is shown, both values are too small to appear in the range of the graph and can be found in Table 1.

concentrations were too low to be detected on flight 16, which is consistent with concentrations found on the other three platforms, as were polluted non-seasalt sulfate concentrations of 3.8 and  $6.5 \mu\text{g m}^{-3}$  on flights 20 and 21 consistent with the range of 4.5 to  $11 \mu\text{g m}^{-3}$  reported for polluted conditions on Punta del Hidalgo and Sagres (Quinn et al., 2000).

### 3.1. Clean marine air

During flights 11 (4 July, JDT 185) and 16 (9 July, JDT 190), the Pelican aircraft sampled clean marine air that had spent several days over the North Atlantic Ocean. Northwesterly winds had transported these clean air masses to the Canary Islands. After transport times of several

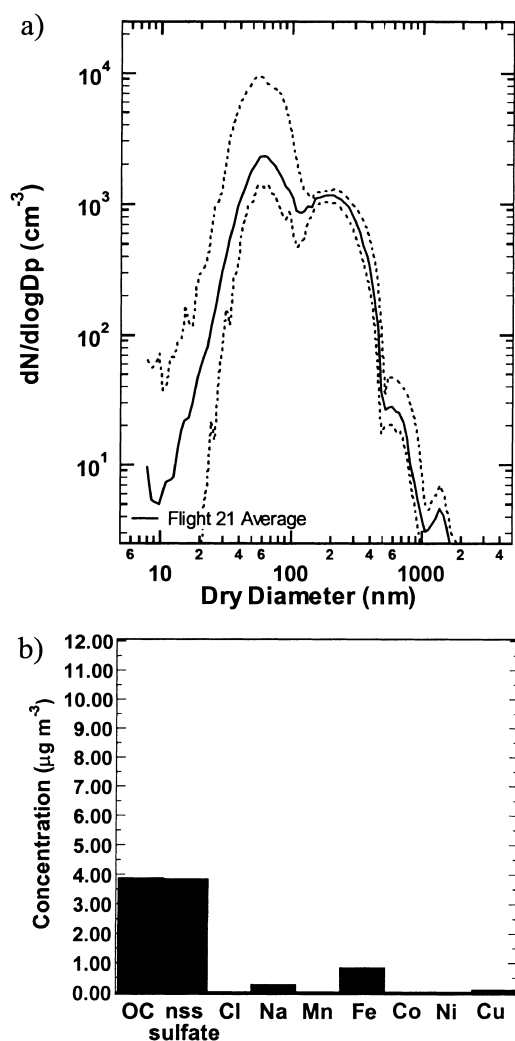


Fig. 3. Aerosol size distributions and chemical compositions for the anthropogenically-influenced case studied, flight 21. Size distributions from integrated ACAD and PCASP measurements are shown in (a) for flight 21. The solid line shows the average value during the filter sampling period for the flight, and the dotted lines give the range of values measured showing the minimum and maximum concentrations with size. Chemical composition data are shown in (b) for flight 21. Filled bars indicate measured values, and empty bars are shown to indicate detection limits. For species where no bar is shown, both values are too small to appear in the range of the graph and can be found in Table 1.

days, the air was well-mixed and contained mainly sea salt and marine components. The sample collected at a single altitude in the boundary layer was likely to be representative of the boundary layer. Figs. 1a, b shows average particle size distributions for each of the 2 clean flights.

The two cases show clearly different concentrations, indicating two types of marine air conditions. Flight 11 is a case with clean marine air characterized by back trajectories that were consistently over the ocean for 5 days before the flight. The large number of particles near 20 nm dry diameter indicates a source of recently-produced particles, although we do not have sufficiently size-resolved chemical composition measurements to distinguish among marine, biogenic, and anthropogenic potential sources. However, in the case of flight 16, the chemical composition indicates that other species were present, including Fe and Cu, which are not typically found in clean marine air (Allen et al., 1997; Brechtel et al., 1998). Back trajectories for flight 16 support this assumption as back trajectories at 3 altitudes from different altitudes in the lower troposphere lead to North Africa and one to Europe. Consequently, we believe that the air mass sampled in flight 16 included some dust-containing or anthropogenically-influenced air masses.

Size distributions show that high concentrations ( $20 \text{ cm}^{-3}$ ) are present in the supermicron part of the measured distribution. These particles may be derived from oceanic (sea salt) or dust sources. Chemical analysis shows that there are small amounts of dust constituents including Fe and Cu present, but these species may also be of anthropogenic origin. Since this sample was collected entirely in the boundary layer and dust particles are usually found predominantly in the free troposphere, these tracers are likely to indicate anthropogenically-influenced air from Europe. These characteristics are consistent with an air mass of mixed origin with some recent sources of anthropogenic particles influencing a predominantly marine particle size distribution.

### 3.2. Dust-laden air

The back trajectories indicate that part of the air mass sampled on flights 15 and 20 (7 and 17 July, or JDT 189 and 199, respectively) originated from North Africa. In addition to oceanic sources, we expect the aerosol particles to consist mainly of



mineral dust derived from the Sahara Desert. In order to obtain more detailed information about the vertical distribution of particulates in this air mass, the aircraft performed flights in spirals down from 3000 m altitude (in the free troposphere) to 60 m altitude (in the boundary layer). In Fig. 2a, b the average size distributions of particles in the part of the free troposphere sampled and in the boundary layer are shown. During aircraft profiles, relative humidity above 1500 m altitude was less than 10% and increased to 70% in the boundary layer. The submicron size distribution above the boundary layer is dominated by a single mode, typical of aerosol size distributions observed in the free troposphere during ACE-2 (Collins et al., 2000). For the particle sizes between 0.9  $\mu\text{m}$  and 1.8  $\mu\text{m}$  dry diameter, where dust particles have been identified previously (Li-Jones et al., 1998), the particle concentrations in these two cases are higher by a factor of 5 or more at concentrations of 10 to 30  $\text{cm}^{-3}$  than in the non-dust cases. Once in the boundary layer the particle size distribution changes and the particle number increases in the fine mode by about an order of magnitude. This change is particularly significant for flight 20, in which some of the boundary layer size distributions may have been influenced by anthropogenic particles from Tenerife.

In the boundary layer, the particle source may be the ocean surface, producing sea salt particles with a peak in concentration at about 2.0  $\mu\text{m}$  due to bubbles bursting at the sea surface. Chemical compositions in flights 15 and 20 are very different from the clean cases and show high amounts of trace metals (Mn, Fe, Co, Ni, Cu). However, in flight 20 Cu has a concentration of 0.071  $\mu\text{g m}^{-3}$ . This high amount of Cu is more indicative of anthropogenic sources than of dust, which is consistent with the high nss sulfate concentration of 6.5  $\mu\text{g m}^{-3}$  during this flight. Back trajectories also indicate an air mass of mixed origin with some back trajectories in this case originating over the European continent. The chemical composition for flight 15 shows high concentrations of trace metals and Na. High amounts of Fe (2.95  $\mu\text{g m}^{-3}$ ) and Mg (5.4  $\mu\text{g m}^{-3}$ ) provide strong indicators for crustal material that has formed dust. Al and Zn were measured as well but showed high blank values resulting from handling and sampling artifacts (the aircraft inlet was made of Al), such that no concentrations for these elements are reported here.

### 3.3. Anthropogenically-influenced air

Some air masses are transported by north-easterly or easterly winds from the European continent to the Canary Islands. Their particle size distributions and compositions are expected to be strongly influenced by anthropogenic emissions. Back trajectories for flight 21 on 18 July (JDT 200) indicate that the observed air mass originated in southwestern Europe. The flight pattern included two circles at two different altitudes (180 m and 60 m) during the aerosol sampling.

In Fig. 3, the average size distribution is shown. Particle size distributions with high concentrations typical of anthropogenically-influenced particles were found including concentrations of more than 5000  $\text{cm}^{-3}$  and a peak dry diameter of 0.06  $\mu\text{m}$ , as shown in Fig. 3a. Many of the particles are present in the accumulation mode, which is typical of anthropogenically-influenced air masses (Hoppel et al., 1990; Russell et al. 1996a). There are also some larger particles, which may originate from either dust or sea salt. Since these measurements were made at low altitudes in the boundary layer, coarse particles in these size distributions are dominated by sea salt.

The chemical composition measured on this flight is also consistent with an anthropogenically-influenced air mass with a small amount of Na (0.29  $\mu\text{g m}^{-3}$ ) and a substantial mass of organic carbon (3.89  $\mu\text{g m}^{-3}$ ), but only minor concentrations of Fe (less than 1  $\mu\text{g m}^{-3}$ ) and Cu (less than 0.2  $\mu\text{g m}^{-3}$ ). Additional evidence for the anthropogenic origin of this air mass is provided by the high nss sulfate concentration (3.85  $\mu\text{g m}^{-3}$ ).

## 4. Comparison with previous atmospheric measurements

Table 2 shows chemical compositions of aerosol particles in several previous studies of ionic and trace metal compositions. Table 2 indicates that our results are in good agreement with results from other field measurements, especially with those performed in the northern Atlantic Ocean.

Na concentration varies significantly with wind conditions in the boundary layer, with our results falling slightly below other reported values. Most Na concentrations in studies with reported surface wind speeds were measured on ship or land-based

Table 2. Concentrations of chemical compounds in fine aerosol particles at a series of locations illustrating clean, dust-containing and anthropogenically-influenced conditions

Concentration [ $\mu\text{g}/\text{m}^3$ ]	Na	Nss sulfate	OC	Mn	Fe	Co	Ni	Cu
ACE-2 Flight 15	0.11	< DL	< DL	0.18	2.95	0.045	0.372	< DL
ACE-2 Flight 16	0.752	< DL	1.1	< DL	0.333	< DL	< DL	0.045
ACE-2 Flight 20	7.8	6.5	< DL	0.036	2.58	< DL	< DL	0.071
ACE-2 Flight 21	0.29	3.8	3.9	< DL	0.851	< DL	< DL	0.108
Bermuda	3.97 <sup>a</sup>	2.65 <sup>b</sup>						
Cape Grim	3.3 <sup>a</sup>							
Hawaii	4.76 <sup>a</sup>							
Heimaey	7.52 <sup>a</sup>							
Mace Head	6.12 <sup>a</sup>	1.94 <sup>b</sup>						
Barbados		1.15 <sup>c</sup>						
S. Ocean		0.033 <sup>d</sup>						
NE. Atlantic		5.16 <sup>c</sup>						
Brisbane			40 <sup>f</sup>	0.092 <sup>f</sup>	2.6 <sup>f</sup>			
Boston				0.088 <sup>g</sup>	3.7 <sup>g</sup>			
Long Beach			39 <sup>g</sup>	0.148 <sup>g</sup>	5.1 <sup>g</sup>			
Kashima				0.02 <sup>h</sup>	4.1 <sup>h</sup>			
Aberg				0.002 <sup>i</sup>	0.037 <sup>i</sup>		0.0037 <sup>i</sup>	0.0002 <sup>i</sup>
Xiang				0.74 <sup>j</sup>	43 <sup>j</sup>	0.52 <sup>j</sup>	0.24 <sup>j</sup>	0.39 <sup>j</sup>
Mexico City				0.07 <sup>k</sup>	1.126 <sup>k</sup>		0.0018 <sup>k</sup>	0.084 <sup>k</sup>
Fuertaventura				0.31 <sup>l</sup>	2.77 <sup>l</sup>			

<sup>a</sup>Gong et al. (1997); <sup>b</sup>Husar et al. (1997); <sup>c</sup>Prospero et al. (1993); <sup>d</sup>Huebert et al. (1998); <sup>e</sup>Hegg et al. (1993); <sup>f</sup>Chan et al. (1997); <sup>g</sup>Thursdon and Spengler (1985); <sup>h</sup>Okamoto et al. (1986); <sup>i</sup>Schmeling (1997); <sup>j</sup>Zhang et al. (1993); <sup>k</sup>Miranda et al. (1994); <sup>l</sup>Bergametti et al. (1989).

stations, located between 5 and 20 m above the sea surface, causing them to reflect higher concentrations than the aircraft measurements (collected above 60 m) due to the rapid settling of coarse particles which results in steep Na concentration gradients above the ocean surface. In addition, Na (and the associated Cl) may be truncated by the upper size cut-off of our inlet since significant sea salt mass can occur above 2.5  $\mu\text{m}$  ambient diameter (Huebert et al., 1998).

Fig. 4 shows trace metal concentrations for flights 15, 16, 20, and 21 with results from several of the studies noted in Table 2. The Shapoutou samples were collected in China during dust storm events and non-dust storm events from the Gobi Desert (Zhang et al. 1993; Zhang et al., 1998). The Fuerteventura sample shows an average value of samples taken with back trajectories from the Sahara Desert (Bergametti et al. 1989). The Aberg study sampled in a non-urban area in western Germany (Schmeling, 1997). Concentrations in these two desert regions have different elemental compositions, but variability within each region makes it difficult to establish definitive character-

istics for each without more measurements. Shapoutou is located in central China and is exposed directly to desert-derived aerosols, whereas air masses reaching the Canary Islands from North Africa have already traveled over the ocean and have mixed with marine air. There are few industries in the Canary Islands, so the anthropogenic contribution to the aerosol is limited compared to central China. Given these limitations we note that dust particles from the Sahara Desert contain more Ni and Zn, but less Fe, Co, Cu and Mn than samples from China. These species are also present in the absence of dust storms in this region, but most of the elemental concentrations (with the exception of Zn) are much lower than during the dust storm periods.

## 5. Chemical effects on aerosol optical properties

For each type of aerosol studied, we want to assess how much the chemical composition of aerosol affects the aerosol optical properties. To

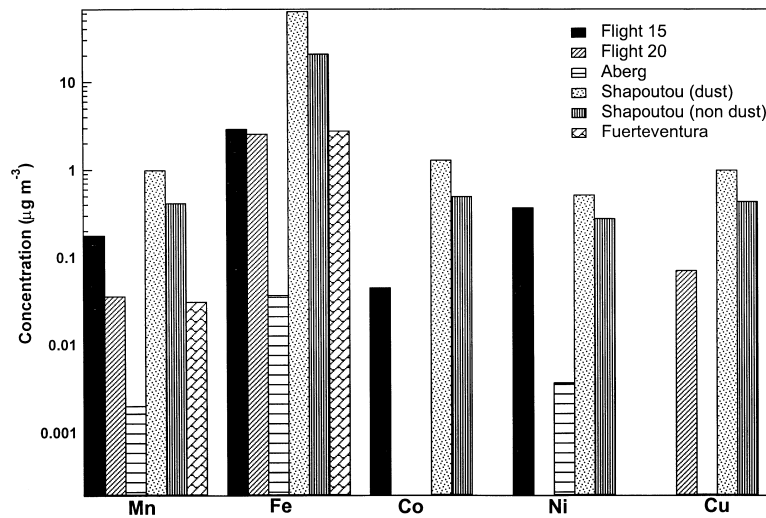


Fig. 4. Trace metal concentrations illustrating concentration differences in anthropogenically and dust-influenced aerosol samples from ACE-2 and other measurement regions. Flights 15 (black bars) and 20 (diagonally-striped bars) are shown from the ACE-2 dust cases. A continental background sample in a non-urban area of a very industrialized region is illustrated by the Aberg sample (horizontally-striped bars) from Schmeling (1997). Data from Zhang et al. (1993; 1998) illustrate concentrations measured in Shapoutou during dust storms (dotted bars) and at other times (vertically-striped bars). The Fuerteventura sample (Bergametti et al., 1989) was taken during a dust event traced back to the Sahara Desert (brick-patterned bars).

answer this question of the role of chemistry in determining the scattering and absorption of light by particles in these five cases studied, we compare the sensitivity of modelled optical properties to differences in particle composition and mixing state.

In order to describe aerosol optical properties, we need to estimate the mass of volatile species associated with the mass collected on the filter, the fraction of mass not identified, and the degree of mixing in the aerosol population. Since the mass of species identified does not account for the total mass present, our approach relies on a model for the aerosol composition which is simplified by assumptions about the unmeasured species. We use the resulting inferred ambient composition to calculate the particle refractive index. From measured values of the ambient relative humidity, we have estimated the fraction of water present in the condensed phase (Howell and Huebert, 1998).

We have used the parameterization proposed by Howell and Huebert (1998) for the general categories of marine and anthropogenically-influenced aerosols to estimate water uptake by the measured dry particle size distribution. Their cor-

relations predict diameter changes of factors from 1.4 to 1.9 corresponding to water mass fractions varying from 30% to 90% at the boundary layer humidity of 80%. In dust cases, filter samples were dominated by the high aerosol accumulation-mode mass in the dust layers sampled. For this reason, optical properties for particle size distributions at low relative humidity that were characteristic of free tropospheric dust layers have been assumed to take up a negligible mass of water (d'Almeida and Schütz, 1983). Using measured compositions of chemical species as indicators of the fractions of sea salt, dust, organic carbon, elemental carbon, and sulfate, the remaining fraction of unidentified dry mass has been assumed to be other soluble ions and has been modeled using the refractive index estimated for dissolved nitrate (d'Almeida et al., 1991).

To calculate the aerosol optical properties, we have converted the chemical compositions in Table 1 into volume fractions of several aerosol types:  $\text{SO}_4^{2-}$  are categorized as "sulfate," OC and EC are each separate types, Cl and Na are grouped together as "sea salt," and Mg, Mn, Fe, Co, Ni, and Cu are grouped together as "dust." For each

flight, the sum of the mass of all species in each aerosol type gives the mass of that type. For a given flight, the amount by which the total mass calculated from the physical size distribution exceeds the measured dry aerosol mass is assigned to the "other" soluble species category, since the refractive indices for several organic and inorganic (such as nitrate) species are similar. Since the scattering properties predicted for these soluble species are similar to water and sulfate and their predicted absorption is negligible, the results are relatively insensitive to the fraction of this "neutral" species present in particles for these calculations. For the non-dust cases, the difference between the total dry aerosol mass and the wet mass derived from the measured ambient size distributions (Collins et al., 2000; Howell and Huebert, 1998) (particles less than 2.5  $\mu\text{m}$  diameter) is assigned to water. In the absence of detailed information on the vapor concentration of HCl, we do not estimate here the potential contribution of this species to the particles. For density, the following approximate values were assumed in the calculation in order to convert the measured mass fraction into a volume fraction for each aerosol type: sulfate 1.78  $\text{g cm}^{-3}$ , OC 1.9  $\text{g cm}^{-3}$ , EC 2.3  $\text{g cm}^{-3}$ , sea salt 2.2  $\text{g cm}^{-3}$ , dust 2.5  $\text{g cm}^{-3}$ , other soluble species 1.78  $\text{g cm}^{-3}$ , and water 1.0  $\text{g cm}^{-3}$ . The resulting approximate models for the different aerosols measured in the five cases studied here are shown in Table 3.

Using the volume percent of each species in each flight given in Table 3, we have calculated internally-mixed average refractive indices for fine particles with spectrally-resolved refractive indices for each component and assuming perfect internal mixing (d'Almeida et al., 1991; Weast et al.,

1985–1986; Hale and Querry, 1973; Toon et al., 1976). Refractive indices of non-absorbing species are mixed assuming volume-weighted mixing (Hänel, 1976) and absorbing species (OC, EC, and dust) are treated with Maxwell-Garnett theory (Bohren and Huffman, 1983).

For comparison, we have also computed the optical properties assuming the aerosol types were externally mixed rather than internally mixed, where the number concentration for each aerosol type with respect to the total size distribution was assumed to be proportional to its volume fraction. Fig. 5a, c shows that refractive indices for clean and anthropogenically-influenced air are practically identical, but for the dust cases refractive indices vary significantly. The similarity in clean and anthropogenically-influenced cases results from the high water content and the lack of elemental carbon (a strong absorber) in all samples. The real part of the refractive index is generally higher for dust cases than for other cases, particularly for wavelengths below 2.0  $\mu\text{m}$ , where dust values exceed 1.5 compared to non-dust cases with values near 1.3 (the value for liquid water). The imaginary part of the refractive index shows the most significant differences at wavelengths above 2.5  $\mu\text{m}$ , where it rises for the clean and anthropogenically-influenced cases to above 0.2 for the liquid water peak.

Refractive indices are then used with particle size distributions to calculate single scatter albedo for the particles below 2.5  $\mu\text{m}$  with a Mie scattering algorithm (Bohren and Huffman, 1983). Single scatter albedos for clean and anthropogenically-influenced cases show similar trends in Fig. 6, corresponding to values near unity and almost no wavelength dependence below 2.5  $\mu\text{m}$ .

Table 3. Fraction of particle volume (given as a % of total submicron ambient particle volume) of each species used to provide representative models of the particle composition for each flight

Flight	Sulfate	OC	EC	Seasalt	Dust	Other	Water
<i>Clean marine cases</i>							
11	0.0	4.1	0.0	0.0	0.0	8.9	87.0
16	1.8	2.7	0.0	3.9	0.7	20.0	70.8
<i>Dust-containing cases</i>							
15	0.0	0.0	0.0	0.8	79.2	20.0	0.0
20	42.7	0.0	0.0	17.9	29.3	10.1	0.0
<i>Anthropogenically-influenced case</i>							
21	22.2	10.4	0.0	0.7	2.0	0.3	64.5

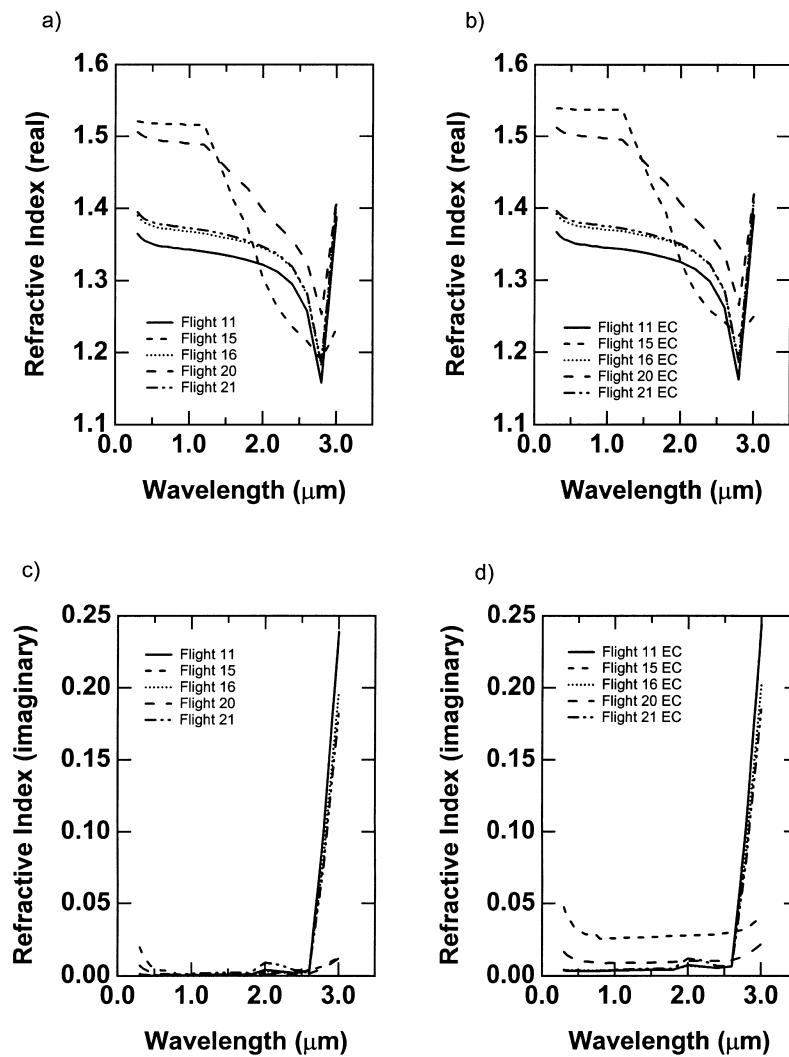


Fig. 5. Refractive indices are shown for the 5 case studies for conditions of clean, dust-laden, and anthropogenically-influenced aerosol flights. Real (a, b) and imaginary (c, d) refractive indices are shown for clean cases — flights 11 (solid line) and 16 (short-dashed line), dust-laden cases — flights 15 (dotted line) and 20 (medium-dashed line), and an anthropogenically-influenced case — flight 21 (long-dashed line). Panels (a) and (c) show the refractive indices for the measured volume composition, and panels (b) and (d) show the results calculated by assuming elemental carbon (“EC”) to be present at the detection limit.

Because of the absorbing properties of dust, dust cases show lower single scatter albedos than non-dust cases below  $0.5 \mu\text{m}$ , reaching as low as 0.8. However, above  $2.5 \mu\text{m}$  where the imaginary part of the refractive index is high in non-dust cases and water begins to absorb strongly, the single scatter albedo decreases drastically to 0.2 and below.

Similarities in the scattering properties of clean and anthropogenically-influenced cases are an expected consequence of the similarities in their components, especially for the water-soluble species whose optical properties are quite similar. Differences in composition obtained from the limited number of samples here suggest few composition-dependent variations in aerosol

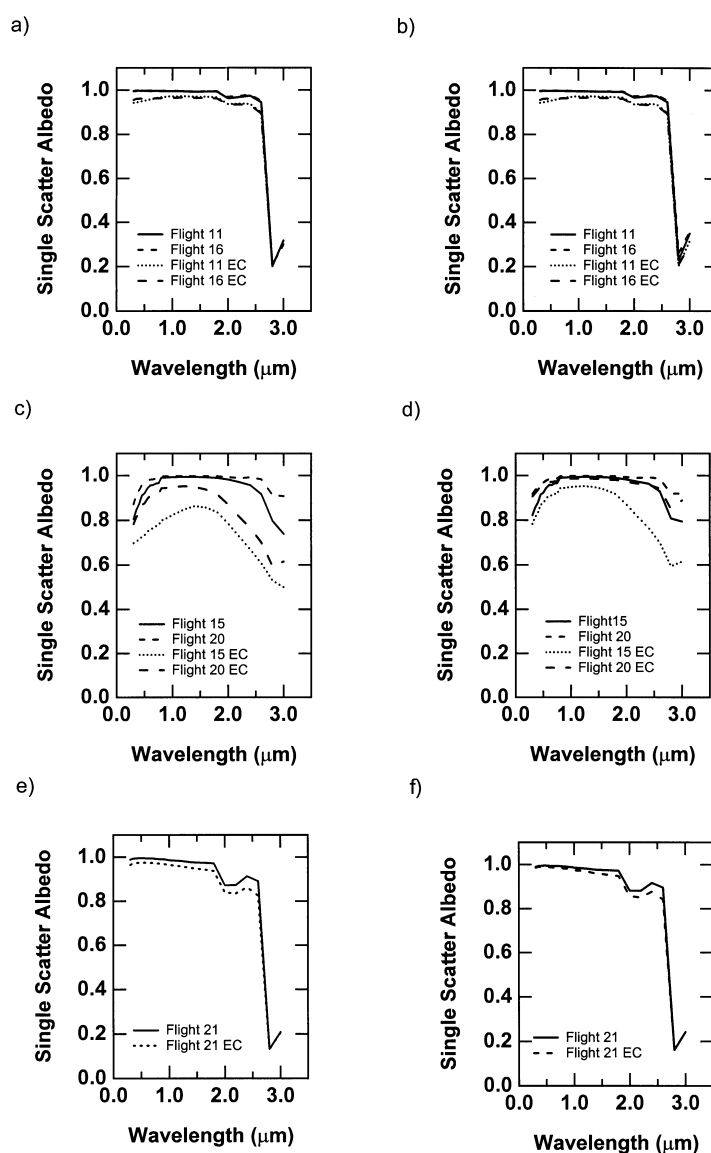


Fig. 6. Single scatter albedo values are shown for the 5 case studies for conditions of clean, dust-laden, and anthropogenically-influenced aerosol. Clean cases during flights 11 and 16 are shown assuming an internal mixture in panel (a) and assuming an external mixture in panel (b). The dust cases for flights 15 and 20 are shown assuming an internal mixture in panel (c) and assuming an external mixture in panel (d). The anthropogenically-influenced case during flight 21 is shown assuming an internal mixture in (e) and assuming an external mixture in (f). For each case, the annotation “EC” denotes the single scatter albedo with the volume fraction of the particle composition modified to include an elemental carbon concentration at the detection limit.

light-absorbing properties for the cases that were not dust-influenced. However, since sampling constraints resulted in detection limits of between 1% and 3% elemental carbon, this apparent similarity

may have resulted from measurement uncertainty. To study the sensitivity of the calculated aerosol properties to this uncertainty, we have used an absorbing carbon content of 0.2% for clean and

2% for anthropogenically-influenced air masses, with the resulting calculated optical properties shown in the curves marked "EC" in Figs. 5, 6. These results illustrate that there is only a modest difference in imaginary refractive index and single scatter albedo in the clean marine and anthropogenically-influenced cases. The imaginary refractive index does increase by an order of magnitude due to the addition of the absorbing EC, and the resulting impact on the single scatter albedo is a decrease from 0.99 to 0.95. Aerosol optical properties in dust cases differ greatly with the amount of absorbing species present, varying with measured fractions of sulfate-to-mineral dust and with the shape of the particle size distributions. Particle number concentration for dust cases also changes markedly at the boundary layer temperature inversion, although aircraft-based data on the associated composition changes were not available.

Direct measurements of in situ optical properties were measured aboard the Pelican with a three-wavelength nephelometer for the two cases showing the largest variation in single scatter albedo, namely the dust-containing flights 15 and 20 (Öström and Noone, 2000). Our estimates of the 550-nm single scattering albedo using internally-mixed, measured-composition (given in Table 3) calculations tend to exceed their values for the dry single scattering albedo that were derived from scattering coefficients measured at 550-nm from the nephelometer and absorption coefficients measured at 565-nm from a particle/soot absorption photometer (Öström and Noone, 2000). For flight 15, our estimates of 0.935 (in the free troposphere) to 0.954 (in the boundary layer) for a profile vertically-averaged from 3881 to 40 m during flight 15 exceeded their measured values of 0.732 (at 3881 m), 0.751 (at 980 m), and 0.806 (at 40 m). However, when we increased the amount of EC to the detection limit for elemental carbon to obtain a lower limit for the single scatter albedo, our estimates were quite similar to those of Öström and Noone (2000) with 0.727 (in the free troposphere) and 0.782 (in the boundary layer). Some of the nephelometer measurements from flight 20 show better agreement with our calculations than those from flight 15. A single scatter albedo of 0.961 was measured at 30 m, as compared to our calculated value for the boundary layer of 0.983. Single scatter albedos of 0.959 and 0.988 were measured at 1918 m and 1916 m,

respectively, as compared to our calculated value for the free troposphere of 0.976. Flight 20 measurements show a large variability in both the free troposphere where they vary from 0.869 at 3885 m to 0.988 at 1968 m and the boundary layer where the measured values vary from 0.805 to 0.961 (Öström and Noone, 2000). Some of the discrepancies in these values are expected, since the filter samples do not identify all components and were collected over time segments different from those used to calculate the average single scatter albedos from the nephelometers. However, the consistent overprediction of our modelled single scatter albedos from the measured calculation suggests that absorbing species (metal or elemental carbon) were present but were not identified in our analysis. The good agreement of the range we predicted by varying the elemental carbon and the mixing state is quite consistent with the measured range, suggesting that within the uncertainties of our calculation, we are in good agreement with the measured values.

## 6. Conclusions

During ACE-2, filter samples of aerosol particles were collected from the Pelican aircraft and were analyzed by three techniques (thermal-optical analysis, ion chromatography, and total reflection X-ray fluorescence), providing detailed aerosol chemical characterizations. Reported concentrations are consistent with those in similar conditions in other studies and illustrate several aerosol types, including clean marine, anthropogenically-influenced, and dust-containing aerosols.

We used measured aerosol chemical composition to assess the importance of aerosol chemistry in determining optical properties among different types of aerosol and for variations within those types. Calculations of associated aerosol optical properties show that the dry dust-laden aerosol are dominated by absorbing mineral components, but missing liquid water absorption. Few differences were predicted between clean marine and anthropogenically-influenced cases despite differences in sulfate and organic carbon fractions, since both were dominated by liquid water properties at high marine boundary layer humidities. These results illustrate the importance of measuring detailed particle composition for dust-containing

cases where the optical properties are especially sensitive to the masses of absorbing species present.

## 7. Acknowledgements

This work was supported by ONR grant N00014-97-1-0673. The Pelican aircraft flight time and instrumentation were supported by NSF grant ATM-9614105. The authors are indebted to Scott Shoemaker for his help in collecting the filter

samples during the Pelican flights and to the CIRPAS crew and Pelican science team for their assistance in the field. The authors are also grateful to Patricia Quinn and Kevin Noone who shared the results of their ACE-2 data in order to make the comparisons referenced in this paper possible. This research is a contribution to the International Global Atmospheric Chemistry (IGAC) Core Project of the International Geosphere-Biosphere Programme (IGBP) and is part of the IGAC Aerosol Characterization Experiments (ACE).

## REFERENCES

- Allen, A. G., Dick, A. L. and Davison, B. M. 1997. Sources of atmospheric methanesulphonate, non-sea-salt sulphate, nitrate and related species over the temperate south Pacific. *Atmos. Environ.* **31**, 191–205.
- Arimoto, R., Duce, R. A., Ray, B. J., Ellis Jr., W. G., Cullen, J. D. and Merrill, J. T. 1995. Trace elements in the atmosphere over the North Atlantic. *J. Geophys. Res.* **100**, 1199–1213.
- Bergametti, G., Gomes, L., Coudegaussen, G., Rognon, P. and Lecoustumer, M. N. 1989. African dust observed over the Canary Islands—source-regions I identification and transport pattern for some summer situations. *J. Geophys. Res.* **94**, 14855–14864.
- Birch, M. E. and Cary, R. A. 1996. Elemental carbon-based method for monitoring occupational exposures to particulate diesel exhaust. *Aerosol Sci. Tech.* **25**, 221–241.
- Bohren, C. F. and Huffman, D. R. 1983 *Absorption and scattering of light by small particles*. John Wiley, New York.
- Brechtel, F. J., Kreidenweis, S. M. and Swan, H. B. 1998. Air mass characteristics, aerosol particle number concentrations, and number size distributions at Macquarie Island during the first Aerosol Characterization Experiment (ACE-1). *J. Geophys. Res.* **103**, 16351–16367.
- Chan, Y. C., Simpson, R. W., Mctainsh, G. H., Vowles, P. D., Cohen, D. D. and Bailey, G. M. 1997. Characterisation of chemical species in PM<sub>2.5</sub> and PM<sub>10</sub> aerosols in Brisbane Australia. *Atmos. Environ.* **31**, 3773–3785.
- Collins, D. R., Jonsson, H. H., Seinfeld, J. H., Flagan, R. C., Gasso, S., Hegg, D., Russell, P. B., Schmid, B., Livingston, J. M., Östrom, E., Noone, K. J., Russell, L. M. and Putaud, J. P. 2000. In situ aerosol size distributions and clear column radiative closure during ACE-2. *Tellus* **52B**, 498–525.
- d'Almeida, G. A., Koepke, P. and Shettle, E. P. 1991. *Atmospheric aerosols: global climatology and radiative characteristics*, A. Deepak, Hampton, Va.
- d'Almeida, G. A. and Schütz, L. 1983. Number, mass, and volume distribution of mineral aerosol and soils of the Sahara. *J. Clim. Appl. Meteorol.* **22**, 233–243.
- Hale, G. M. and Querry, M. R. 1973. Optical constants of water in the 200-nm to 200  $\mu$ m wavelength region. *Applied Optics* **12**, 555–563.
- Hänel, G. 1976. The properties of atmospheric aerosol particles as functions of the relative humidity at thermodynamic equilibrium with the surrounding moist air. *Adv. Geophys.* **19**, 73–188.
- Hegg, D. A., Ferek, R. J. and Hobbs, P. V. 1993. Light scattering and cloud condensation nucleus activity of sulfate aerosols measured over the Northeast Atlantic ocean. *J. Geophys. Res.* **98**, 14887–14894.
- Hoppel, W. A., Fitzgerald, J. W., Frick, G. M., Larson, R. E. and Mack, E. J. 1990. Aerosol size distributions and optical properties found in the marine boundary layer over the Atlantic Ocean. *J. Geophys. Res.* **95**, 3659–3686.
- Howell, S. G. and Huebert, B. J. 1998. Determining marine aerosol scattering characteristics at ambient humidity from size-resolved chemical composition. *J. Geophys. Res.* **103**, 1391–1404.
- Huebert, B. J., Zhuang, L., Howell, S., Noone, K. and Noone, B. 1996. Sulfate, nitrate, methanesulfonate, chloride, ammonium, and sodium measurements from ship, island, and aircraft during the Atlantic Stratocumulus Transition Experiment/Marine Aerosol Gas Exchange. *J. Geophys. Res.* **101**, 4413–4423.
- Huebert, B. J., Howell, S. G., Zhuang, L., Heath, J. A., Litchy, M. R., Wylie, D. J., Kreidler-Moss, J. L., Coppicus, S. and Pfeiffer, J. E. 1998. Filter and impactor measurements of anions and cations during the first Aerosol Characterization Experiment (ACE 1). *J. Geophys. Res.* **103**, 16493–16509.
- Husar, R. B., Prospero, J. M. and Stowe, L. L. 1997. Characterization of tropospheric aerosols over the oceans with the NOAA advanced very high resolution radiometer optical thickness operational product. *J. Geophys. Res.* **102**, 16889–16909.
- Klockenkämper, R. 1997. *Total reflection X-ray fluorescence analysis*, ed. J. D. Winefordner. John Wiley and Sons, New York, 245 pp.



- Li-Jones, X. and Prospero, J. M. 1998. Variations in the size distribution of non-sea-salt sulfate aerosols in the marine boundary layer at Barbados: impact of African dust. *J. Geophys. Res.* **103**, 16073–26084.
- Miranda, J., Cahill, T. A., Morales, R. J., Adalpe, F., Flores, M. J. and Diaz, R. V. 1994. Determination of elemental concentrations in atmospheric aerosols in Mexico City using proton induced X-ray emission, proton elastic scattering and laser absorption. *Atmos. Environ.* **28**, 2299–2306.
- Okamoto, S., Kobayashi, K. and Yamada, T. 1986. Characterisation of aerosols in the Kashima area and a source apportionment study. In: *Sydney Clean Air Congress 1986*, pp. 253–262.
- Öström, E. and Noone, K. J. 2000. Vertical profiles of aerosol scattering and absorption measured in situ during the North Atlantic Aerosol Characterization Experiment. *Tellus* **52B**, 526–545.
- Prospero, J. M., Savoie, D. L., Arimoto, R. and Huang, F. 1993. Long-term trends in mineral dust concentrations over the western North Atlantic: Relationship to North African rainfall. *Eos Trans. AGU* **74**, Fall Meeting Suppl.
- Putaud, J. P., Van Dingenen, R., Mangoni, M., Virkkula, A., Raes, F., Maring, H., Prospero, J. M., Swietlicki, E., Berg, O. H., Hillamo, R. and Makela, T. Chemical mass closure and origin assessment of the submicron aerosol in the marine boundary layer and the free troposphere at Tenerife during ACE-2. *Tellus* **52B**, 141–168.
- Quinn, P.K., Coffman, D.J., Bates, T.S., and Covert, D.S. 2000. A comparison of aerosol chemical and optical properties from the first and second Aerosol Characterization Experiments. *Tellus* **52B**, 239–257.
- Raes, F., Bates, T. S., McGovern, F. M. and Van Liedekerke, M. 2000. The second Aerosol Characterization Experiment (ACE-2): General overview and main results. *Tellus* **52B**, 111–125.
- Russel, P. A. and Heintzenberg, J. 2000. Clear Column Experiments in ACE-2. *Tellus* **52B**, 463–483.
- Russell, L. M., Huebert, B. J., Flagan, R. C. and Seinfeld, J. H. 1996a. Characterization of submicron aerosol size distributions from time-resolved measurements in the Atlantic stratocumulus transition experiment/marine aerosol and gas exchange. *J. Geophys. Res.* **101**, 4469–4478.
- Russell, L. M., Stolzenburg, M. R., Caldow, R., Zhang, S. H., Flagan, R. C. and Seinfeld, J. H. 1996b. Radially-classified aerosol detector for aircraft-based submicron aerosol measurements. *J. Atmos. Ocean. Tech.* **13**, 598–609.
- Schmeling, M. 1997. *Anwendung der Totalreflexions-Röntgenfluoreszenz zur Analyse von luftgetragenen Partikeln*. PhD-thesis, Dortmund, 77 pp.
- Schmeling, M. and Klockow, D. 1997. Sample collection and preparation for analysis of airborne particulate matter by total reflection X-ray fluorescence spectrometry. *Anal. Chim. Acta* **346**, 121–126.
- Schütz, L. and Seibert, M. 1987. Mineral aerosols and source identification. *J. Aerosol Sci.* **18**, 1–10.
- Seinfeld, J. H. 1986. *Atmospheric chemistry and physics of air pollution*. John Wiley and Sons, New York, 738 pp.
- Streli, C. 1997. Total reflection X-ray fluorescence analysis of light elements. *Spectrochim. Acta* **52B**, 281–293.
- Swietlicki, E., Zhou, J., Berg, O. H., Hameri, K., Vakeva, M., Makela, J., Covert, D. S., Dusek, U., Busch, B., Wiedensohler, A. and Stratmann, F. 2000. Hygroscopic properties of aerosol particles in the Northeastern Atlantic during ACE-2. *Tellus* **52B**, 201–227.
- Thursdon, G. D. and Spengler, J. D. 1985. A quantitative assessment of source contributions to inhalable matter pollution in metropolitan Boston. *Atmos. Environ.* **19**, 9–25.
- Toon, O. B., Pollack, J. B. and Khare, B. N. 1976. The optical constants of several atmospheric aerosol species: ammonium sulfate, aluminum oxide, and sodium chloride. *J. Geophys. Res.* **81**, 5733–5742.
- Verver, G., Raes, F., Vogelesang, D. and Johnson, D. 2000. The second Aerosol Characterization Experiment (ACE-2). Meteorological and chemical context. *Tellus* **52B**, 126–140.
- Weast, R. C., Astle, M. J. and Beyer, W. H. (Eds.) 1985–1986. *CRC Handbook of chemistry and physics*, 66th edition. CRC Press, Boca Raton, Fla., p. D-233.
- Zhang, X., Arimoto, R., An, Z., Chen, T., Zhang, G., Zhu, G. and Wang, X. 1993. Atmospheric trace elements over source regions for chinese dust: Concentrations, sources and atmospheric deposition on the Loess Plateau. *Atmos. Environ.* **27**, 2051–2067.
- Zhang, X. Y., Arimoto, R., Zhu, G. H., Chen, T. and Zhang, G. Y. 1998. Concentration, size distribution and deposition of mineral aerosol over Chinese desert regions. *Tellus* **50B**, 317–330.